

# Animated Stickies: Fast Video Projection Mapping onto a Markerless Plane through a Direct Closed-Loop Alignment

Shingo Kagami, *Member, IEEE*, and Koichi Hashimoto, *Member, IEEE*

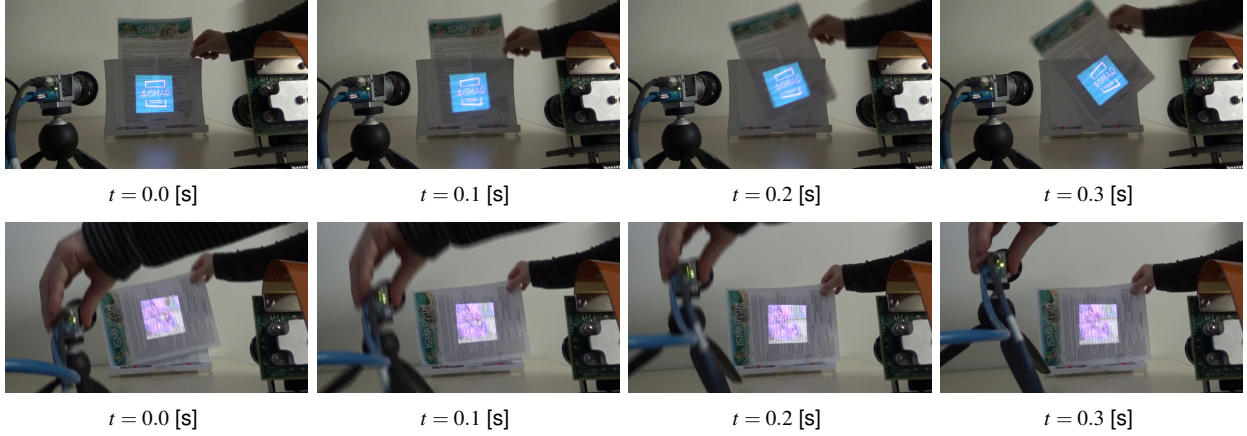


Fig. 1. Snapshot sequences of dynamic projection mapping onto fast moving markerless surfaces. The bottom row indicates that moving the camera pose (left side in the photo) relative to the projector (right side) does not disturb the mapping.

**Abstract**—This paper presents a fast projection mapping method for moving image content projected onto a markerless planar surface using a low-latency Digital Micromirror Device (DMD) projector. By adopting a closed-loop alignment approach, in which not only the surface texture but also the projected image is tracked by a camera, the proposed method is free from a calibration or position adjustment between the camera and projector. We designed fiducial patterns to be inserted into a fast flapping sequence of binary frames of the DMD projector, which allows the simultaneous tracking of the surface texture and a fiducial geometry separate from a single image captured by the camera. The proposed method implemented on a CPU runs at 400 fps and enables arbitrary video contents to be “stuck” onto a variety of textured surfaces.

**Index Terms**—Spatial augmented reality, high-speed vision, projector-camera system, visual tracking

## 1 INTRODUCTION

The successful implementation of spatial augmented reality (SAR) in dynamic scenarios necessitates the use of fast low-latency projection systems that can adapt images quickly to scene motions. State-of-the-art systems utilize Digital Micromirror Device (DMD) projectors to update projected images at several hundreds of fps or higher [6, 13, 15, 20, 23].

These systems may seem too costly today in terms of price, system size, and operational cost to be used for consumer-level applications. However, considering that DMD projectors in general are the most popular choice for mobile and pico-projectors and that the core optical engines of low-latency systems are the same as those used in regular DMD products, the widespread use of commercial low-latency projectors in the future may be a possibility. Recalling that some popular smartphones are already equipped with high-speed (e.g., 240 fps) cameras, addressing the issue of how to realize a casual consumer-level use of low-latency SAR systems is important.

For such casual use, SAR systems should consist of a minimal number of components and should be easy to set up. For example, it is desirable to avoid attaching markers on the target surfaces, as well as a precise adjustment of the camera-projector positions and their calibration.

Image alignment techniques for augmented reality are generally classified into two approaches: closed- and open-loop. Closed-loop

approaches [1, 12, 13, 21, 22, 26, 33] track not only the target surface but also the projected pattern to minimize alignment errors, and are therefore insensitive to, and occasionally almost free from, positioning or calibration errors.

Most existing low-latency SAR systems employ open-loop approaches to avoid projection pattern tracking, presumably owing to a limited computation time budget. A popular tracking measure is the use of infrared cameras, by which the projected patterns are not observed. Narita et al. [23] used markers drawn on a surface using infrared-absorbing ink for tracking. Bermano et al. [6] tracked a markerless human face illuminated by infrared light. Both used coaxially aligned projector-camera pairs allowing 3D position measurements to be avoided. However, the alignment of the optical axes requires a careful operation and may not be fit for casual use.

When we do not limit the discussion to cases using low-latency projectors, the most popular choice for tracking in dynamic SAR applications in the recent literature would be the use of depth sensors [27, 35]. Because depth information is not affected by the projected content, this approach is classified as open-loop unless other sensory information is adjunctively used. Therefore, errors in 3D modeling and sensor calibration, for example, inevitably affect the results. It is also challenging to achieve low-latency sensory feedback with depth sensors when compared to the use of 2D cameras.

The closed-loop approach, by contrast, is a challenge owing to the difficulty of target surface tracking under interference by the projected content. A front door approach tackles this issue by incorporating the effect of projection into the optimization process for alignment purposes [1, 2, 22, 33]. Adopting this approach to real-time tracking at

- Shingo Kagami is with the Graduate School of Information Sciences, Tohoku University. E-mail: swk(at)ic.is.tohoku.ac.jp.
- Koichi Hashimoto is with the Graduate School of Information Sciences, Tohoku University.

a high frame rate, however, is difficult mainly because the optimization problem becomes complicated and intractable when the frame time is short. When a video content, instead of a still image, is projected, the complexity increases because the template image for tracking changes and must be initialized every frame. The dependency of the tracking accuracy on the projection content is also problematic. When the tracker comes across a featureless video frame, the tracking result will become suddenly unstable.

Researchers occasionally have avoided this interference by limiting their target to a texture-less solid-color surface. Johnson and Fuchs [12] and Resch et al. [26] assumed a texture-less non-planar surface with a known shape, and tracked the known feature points in the projected image reflected by the surface to determine the projector pose. Kagami and Hashimoto [13] assumed a white planar quadrangle surface, and tracked the projected image through a direct alignment and tracked the four sides of the quadrangle by line fitting to the edges. In all cases, the problem of dependency on the projection contents remains to be solved.

This problem of content dependency can be eliminated if we hide imperceptible fiducial patterns in a projected video sequence, allowing the tracking of patterns to be geometrically equivalent to the tracking of the projection content. A popular and classical approach to this is to insert additional frames into the projection content [7, 11, 17, 19, 25]. Because DMD projectors represent an image through a sequence of fast switching binary frames, it is possible to make the inserted frames so short that the human eyes can barely perceive them.

However, even with this fiducial-hiding approach, we also need to face the interference problem. For a static scene, it may be possible to suppress the interference by processing multiple consecutive frames. For example, by consecutively capturing a pattern frame and its complementary-color frame, the pattern geometry can be extracted from their difference [10, 32] and possibly recover the surface texture from their average. For a highly dynamic scene, however, this will not work. The use of an infrared pattern projection [31] or image steganographic method [29] will not help in this regard.

In this light, we address the issue of tracking the surface texture and projected fiducial patterns separately from a single camera frame. Our approach is to make use of the spatial domain for separation under the strong assumption of a high frame rate measurement. Thanks to its closed-loop configuration, the proposed method is free from a camera-projector calibration.

This paper focuses on the planar target surfaces primarily because the hardware platform we use [15] supports only a homography transformation with hard-wired logic implemented in the projector. It should be noted, however, that focusing on the planar targets is not only a simplification but incurs a peculiar difficulty and profound significance. For example, the lack of 3D shape features prevents the use of existing techniques relying on 3D information. From a practical perspective, planar or approximately planar surfaces are in great demand as projection targets. The possibility of generalization to non-planar surfaces is discussed in Sect. 7.

## 2 PROJECTION SYSTEM

This section describes the hardware platform [15] upon which the proposed method is implemented. This DMD projection system has been designed to enable low-latency mapping of video-rate content onto a moving surface without the need for generating content with a high frame rate. Note, however, that the proposed method itself will be applicable to a wider class of high-speed projectors.

A DMD is a reflective spatial light modulator that produces monochrome binary images at up to tens of kilohertz. Fast switching  $2^n - 1$  binary images are time-averaged by the human eye and perceived as an  $n$ -bit gray-level image. With a light source whose brightness can be modulated for each binary frame, the necessary number of binary frames can be reduced, which is the principle that most high-speed DMD projectors are based upon.

Our system adopts a different approach. Instead of increasing the frame rate of the video content and thereby achieving a low-latency motion adaptation, it warps each of the binary frames at the binary

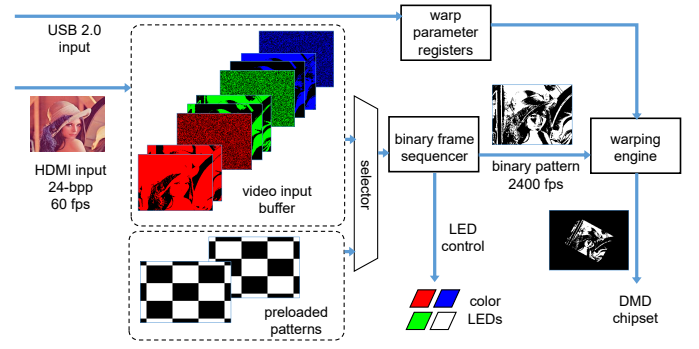


Fig. 2. Operation pipeline of our projection system.

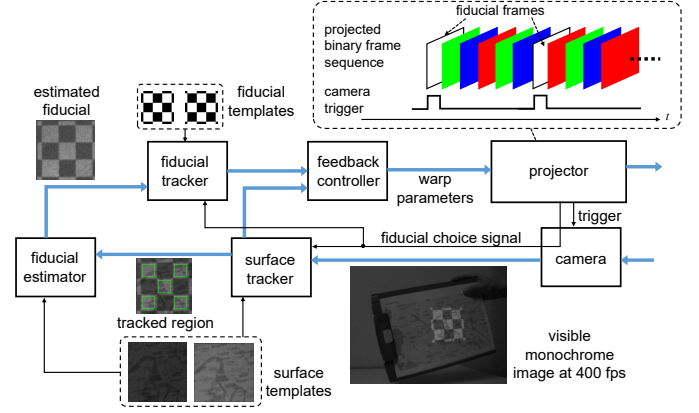


Fig. 3. Pipeline of the proposed method.

frame rate. Oshiro et al. [24] reported that applying this technique to 60-fps images offers a perceptual image quality comparable to that of high frame rate images. Similar approaches have been proposed for head-mounted displays [18, 34], where binary frames are generated at every time instant; however, our approach is simpler in that binary frames are simply selected instead of being generated. Microsoft HoloLens, using liquid crystal on silicon (LCoS) instead of DMD, also applies a similar technique to each color field [16].

Fig. 2 shows the pipeline of the projection system. It receives a 24-bpp 60-fps video stream through HDMI and decomposes a frame into bitplanes. Binary patterns are read out at a binary frame rate of up to 2,470 fps from this input bitplane buffer or a storage of preloaded binary patterns according to a predefined sequence. A binary pattern is warped according to the homography parameters that have been received most recently through a USB 2.0 port, and sent to a 0.7" XGA DMD (Texas Instruments DLP7000BFLP). The sequencer also controls RGB-White LEDs (Luminus SBM-40) that illuminate the DMD, and the light reflected by the DMD travels through the projection optics (ViaLUX STAR CORE-07).

It is notable that there is no need for high frame rate video input, which leads to a low-cost implementation suitable for consumer-level products. Another advantage of this approach is that the binary pattern rate used to represent color images can be kept relatively low (i.e., a few instead of tens of kilohertz), which allows the use of a lower-cost DMD and simplified electronics design.

## 3 FIDUCIAL DESIGN AND PLANE TRACKING METHOD

Fiducial patterns should be inserted into the binary frame sequence as frequently as required for sensor feedback, and should have the following properties:

- imperceptibility (or hardly perceptible) by human eyes;
- no disturbance of the surface texture tracking;

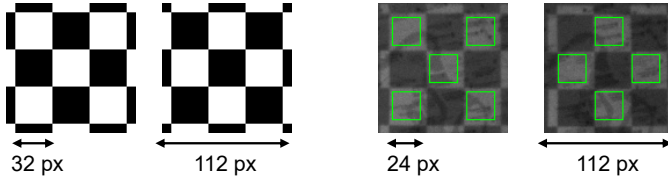


Fig. 4. Fiducial design (left) and corresponding area of interest of a surface (right) warped to the template size of the surface tracker. Only the pixels in the green rectangles are used in the direct alignment algorithm.

- recoverability of geometry from a single frame measurement.

For the imperceptibility, the display period of the pattern must be sufficiently short. When DMD projectors are used, it means the pattern should be a binary or superposition of a few binary images. To avoid the time-integration of the patterns, which repeatedly appear at the sensor feedback rate, from being visible, complementary-color pairs of patterns should be displayed with equal occurrence frequency.

For surface tracking to be executed at a high frame rate with a relatively low computational cost, we focus on direct alignment methods, which directly minimize the differences of the pixel values without an explicit feature extraction. It is well known that direct alignment methods work well even if only a selected subset of the pixels are used during optimization, the popular choices of which are a random selection or high curvature texture points [3, 8].

This motivates us to select camera image pixels illuminated by bright pixels in the fiducial binary pattern displayed by the projector and let them participate in the optimization. The issue faced here is that it is unknown which pixels in the camera image are illuminated and which pixels are not, which is the very goal of optimization.

Therefore, we make a strong assumption that tracking in the previous camera frame is successful and that inter-frame motion between the consecutive camera images is sufficiently small thanks to high frame rate measurements. We propose the use of chessboard-like patterns and select those pixels that lie in *eroded* regions of white chessboard cells in the previous camera frame. Because we assume that inter-frame motion is small, we are sure that most of these pixels are also illuminated by the white chessboard cells in the current camera frame.

The next problem is to locate the fiducial pattern in the current camera frame. Under the assumption that we have already tracked the surface texture successfully, it is reasonable to consider the reflectance of the surface at each camera pixel as equal to that of the corresponding pixel measured when initialization of the tracking is conducted. This information can be used to classify whether a pixel of interest is illuminated by the chessboard white cell.

More specifically, during the initialization phase, we store an image  $I^+$  of the tracked regions of the surface with all projector pixels on, and another image  $I^-$  with all pixels off, and memorize the mean pixel values  $\bar{I}^+$  and  $\bar{I}^-$  of both images.

During the tracking phase, we seek a uniform gain coefficient multiplied with the pixel values in the tracked regions such that their mean becomes equal to the memorized  $\bar{I}^+$ . After we obtain the pixel-wise correspondence between the input image and the memorized  $I^-$  by completing the surface tracking, the pixel values are normalized by dividing them by the corresponding pixel values in  $I^-$ . This normalized image is now expected to have a value close to  $\bar{I}^+/\bar{I}^-$  at a pixel illuminated by the chessboard white cells, and a considerably lower value otherwise. This normalized image is treated as an input to another direct alignment process against the fiducial template image. Although this normalization is only an approximation, it works sufficiently well for a direct alignment against the binary-valued fiducial templates.

The exception is a case in which the ambient light is too low, where division by  $I^-$  values is unreliable. In this case, namely, when  $\bar{I}^-$  is less than 16 at an 8-bit level, our implementation simply uses the gain-adapted surface tracking result as the input to the fiducial tracking process.

Fig. 3 illustrates the pipeline of the proposed method. We set the

binary frame rate to 2,400 fps and insert the fiducial patterns such that they appear in every sixth binary frame, resulting in a 400-fps visual feedback rate. A trigger signal is sent from the projector to a Basler USB-3 monochrome camera acA640-750um to control the shutter, along with a binary signal indicating whether the original fiducial pattern or its complementary pattern is presented. Whereas the proposed method does not depend on a specific choice of direct alignment methods, we chose the efficient second-order minimization (ESM) method [5] for both surface and fiducial tracking because it has been found to work well for the tracking of content projected onto a plane [13].

The design of the fiducial pattern is crucial in achieving high accuracy tracking. In our initial attempt, we attempted the use of simple  $3 \times 3$  chessboard patterns, although the resulting accuracy of the fiducial positioning was far from satisfactory. Because only the borders of the chessboard cells provide information to position the fiducial in the image, they should appear as close as possible to the peripheries of the video content area. By contrast, overly fine chessboard grids make the surface tracking difficult. We chose a pattern that is marginally larger than the  $3 \times 3$  chessboard shown in Fig. 4.

The light source setting for the fiducial pattern projection is also important. On the one hand, in order to keep the visible color contrast of the presented content sufficiently high, the illumination intensity for the fiducial should be as low as possible and the illumination period should be as short as possible. On the other hand, the illumination for the fiducial must provide a sufficient light amount for the short-exposure camera measurement of the patterns to be reliable. This tradeoff must be dealt with by considering many factors including the surface reflectance and ambient light, and is manually adjusted in our current implementation. A white light source color is chosen (or if a white light source is unavailable, all RGB values are turned on) because it is a neutral color for various types of spectral surface reflectance.

## 4 TRACKING PROJECTION ALGORITHM

### 4.1 Initialization

For initialization, a user-specified rectangle is given in the projector image space. During the initialization phase, the projector inserts a white frame, a black frame, an ArUco marker frame [9], and an intensity-inverted counterpart of the ArUco marker frame in place of the chessboard-like fiducials used in the tracking phase, into the video sequence. When the user issues a command to start tracking, the camera captures these four consecutive frames and tries to detect the ArUco marker position by binarizing the marker frame with the pixel-wise threshold given by the average intensity of the white and black frames. If the detection fails, the next four consecutive frames are captured and the same procedure is repeated.

Once detected, the four corners of the projected ArUco marker are used to determine the surface area onto which the projected content is mapped. In our implementation, four corners of the quadrangle area are used as control points to specify the area, which are called the *surface corners* in the rest of the paper. Note that these are only imaginary points acting as anchors for control and need not correspond to feature-rich points in the surface texture. The template images  $I^+$  and  $I^-$  are then sampled from this area.

### 4.2 Tracking Control

During the tracking phase, after capturing each newest camera frame, the tracking procedure described in Sect. 3 is executed using the surface corners in the previous frame applied as the initial values for the optimization. This procedure outputs the tracking results of the surface corners and the *fiducial corners*, which are defined as control points in the fiducial pattern that should coincide with the surface corners.

From the tracked fiducial corner coordinates in the camera image space and the known fiducial corner coordinates in the projector image space, we obtain a homography matrix  $H_{pc}$  with respect to the surface plane to map a camera image point to its corresponding projector image point. By mapping the surface corners into the projector image space using this homography matrix, we have the four goal points toward which the fiducial corners are regulated in the projector image space.



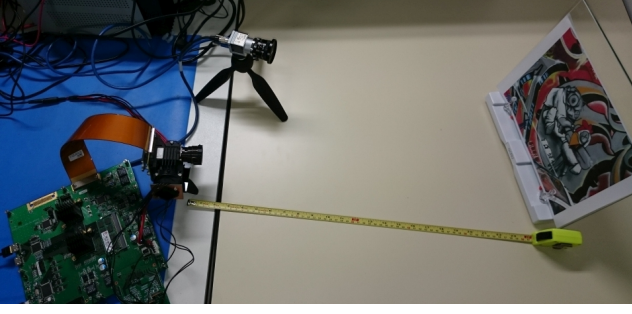


Fig. 5. Overview of evaluation setup.

For this control, Kagami and Hashimoto [13] applied a simple proportional-derivative (PD) controller to each of these four corners. Although they demonstrated that this achieves a fairly good tracking performance when a solid-color surface is used as a target, small tracking errors caused by the feedback-only control can cause a perceptible misalignment when a textured target surface is used. Therefore, we introduce a simple implementation of the Smith predictor. In general, a control system using the Smith predictor for a discrete time system is given by [30]:

$$\begin{aligned} u(z) &= C(z)e(z) \\ e(z) &= y_d - y + (z^{-k} - 1)G(z)u(z) \end{aligned}$$

where  $u$  is the output of the controller  $C$ ,  $e$  is the error input to the controller,  $G$  is the plant model,  $y$  and  $y_d$  are the observed (i.e. fiducial corner position) and desired (i.e. surface corner position) outputs, respectively, and  $z^{-k}$  is the delay operator with dead time  $k$  [camera frames]. Using a PD controller  $C(z) = K_p + K_d(1 - z^{-1})$  which takes the position error as input and generates the velocity output of a corner point, a simplest plant model is the pure integrator  $G(z) = \sum_{n=1}^{\infty} z^{-n}$ , meaning that the unknown motion of the target surface is simply neglected. Plugging these definitions into the above equations yields

$$\begin{aligned} u(z) &= \{K_p + K_d(1 - z^{-1})\}e(z) \\ e(z) &= y_d - y - \sum_{n=1}^k z^{-n}u(z). \end{aligned}$$

This means that we only need to memorize the recent  $k$  outputs from the PD controller and to add their sum to the observed fiducial corner position  $y$ .

In our implementation, dead time  $k = 1$  was chosen because even an extremely small  $K_p$  with  $K_d = 0$  cannot stabilize the system when the dead time is set to  $k = 2$ . This suggests that the overall system latency is longer than 1 camera frame and shorter than 2 camera frames (i.e., between 2.5 and 5.0 ms). The controller gains were empirically chosen to be  $K_p = 0.15$  and  $K_d = 4.0$ .

Once the values of  $u$  are computed for the four corners, they are added to the current fiducial corner positions in the projector image space to determine the next fiducial corner positions. The homography matrix for the projected content is computed from these positions and sent to the projector.

## 5 QUANTITATIVE EVALUATION

Our goal is to achieve a mapping of the projected contents onto a fast and randomly moving surface; however, it is difficult to evaluate the performance of such a system quantitatively, mainly because the accurate ground truth is difficult to obtain. However, a simulation using synthesized images does not consider the various sources of a disturbance.

We therefore decided to prepare many real images of fixed surfaces onto which randomly warped fiducial patterns are projected, and run the tracking algorithm from randomly deviated initial surface corner points from the ground truth to see if the results converge with the ground truth.

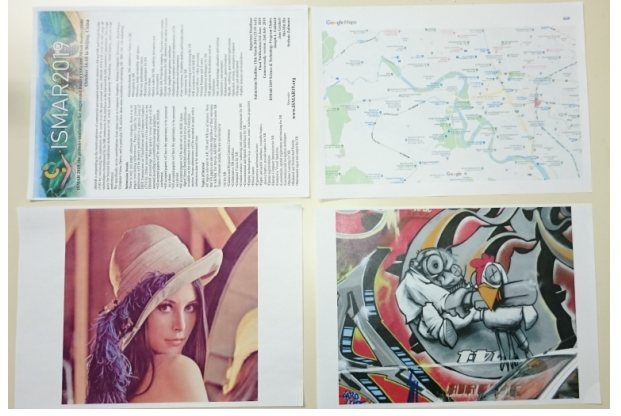


Fig. 6. Target surfaces used for evaluation.

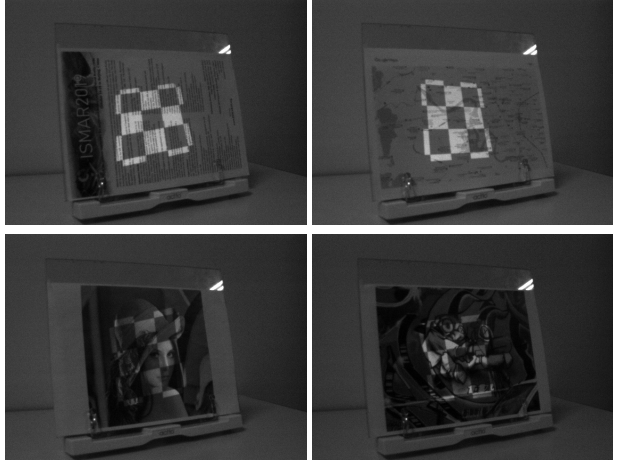


Fig. 7. Examples of captured images in the evaluation test.

### 5.1 Dataset Acquisition

We ran the proposed method for a fixed surface set in front of the projector-camera system and made sure that it converged to seemingly correct positions through an eye observation. The surface corner positions tracked in the camera image space at this time instant were stored as the *ground truth surface corner points*, which are common for all the images taken with this surface.

At the same time, the fiducial corner positions tracked in the camera image space and the known fiducial corners in the projector image space were used to estimate the homography matrix  $\hat{H}_{pc}$  with respect to this surface.

To generate randomly warped fiducial patterns, random numbers drawn from a normal distribution  $N(0, \sigma_f^2)$  were added to the ground truth surface corners to generate the *ground truth fiducial corner points*. These corner points were mapped by  $\hat{H}_{pc}$  to the projector image space to control the projector such that the corners of the projected fiducial patterns were observed in the camera image at the above-defined ground truth fiducial corners. The camera images of this scene were captured 100 times for each of  $\sigma_f = 1, 2, 4, 8$  [pixels] with each of the original fiducial patterns and their inverted counterparts. In addition, 100 images with all projector pixels on, and another set of 100 images with all pixels off, were captured and stored. This entire procedure was repeated for four surfaces with different textures: “Text,” “Map,” “Lenna,” and “Graffiti,” each of which was printed on a sheet of copier paper using a color laser printer and stuck onto a glass plate.

Fig. 5 shows the evaluation setup. Images with a pixel resolution of  $640 \times 480$  were taken using a Basler acA640-750um camera with the exposure time set to  $400 \mu s$  and the gain set to 16, through a Space

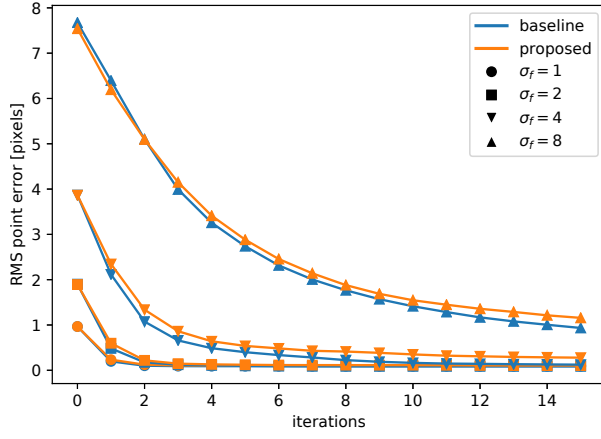


Fig. 8. Average RMS point errors of surface tracking versus iteration count when no projection interference takes place.

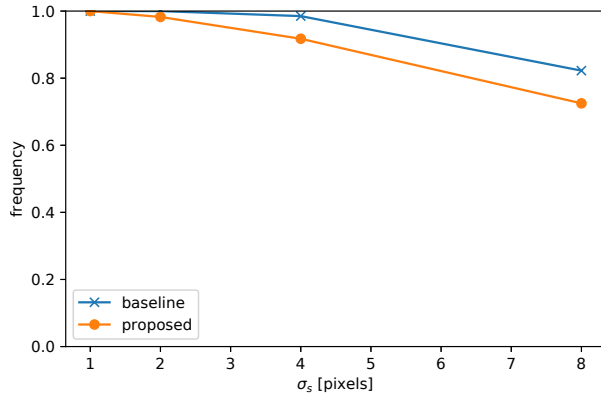


Fig. 9. Frequency of convergence of surface tracking when no projection interference takes place.

HF3.5M-2 C-mount lens (3.5-mm focal length, F1.6). Illuminance at around the surface was approximately 210 lx, and the pixel value of a white surface point was approximately 60 when not illuminated by the projector and approximately 150 when illuminated by the white light source used to present the fiducials. Fig. 6 shows the four surfaces used for the evaluation and Fig. 7 presents examples of the captured images.

## 5.2 Tracking Test Procedure

Using the above dataset, off-line optimization tests were carried out with randomly deviated initial values to see the performance with respect to the convergence rate of optimization and how frequently the optimization converged. Random numbers drawn from  $N(0, \sigma_s^2)$  were added to the ground truth surface corners to generate the initial corner points from which optimization begins.

We carried out 100 trials of optimization for each combination of the optimization methods, four surface types, two patterns of fiducials,  $\sigma_f = 1, 2, 4, 8$  [pixels], and  $\sigma_s = 1, 2, 4, 8$  [pixels]. During each trial, an image with all projector pixels on, another with all projector pixels off, and a third with the fiducial pattern retrieved randomly from the dataset were applied. The template images  $I^+$  and  $I^-$  were sampled from the first two images, respectively, from the quadrangle specified by the ground-truth surface corners. The other image is used to test the tracking algorithm from the initial corner positions with  $\sigma_s$  deviations. For the optimization methods, we applied both the plain ESM method as the baseline and the proposed method. The number of iterations for both methods was limited to 15 for surface and fiducial tracking, respectively.

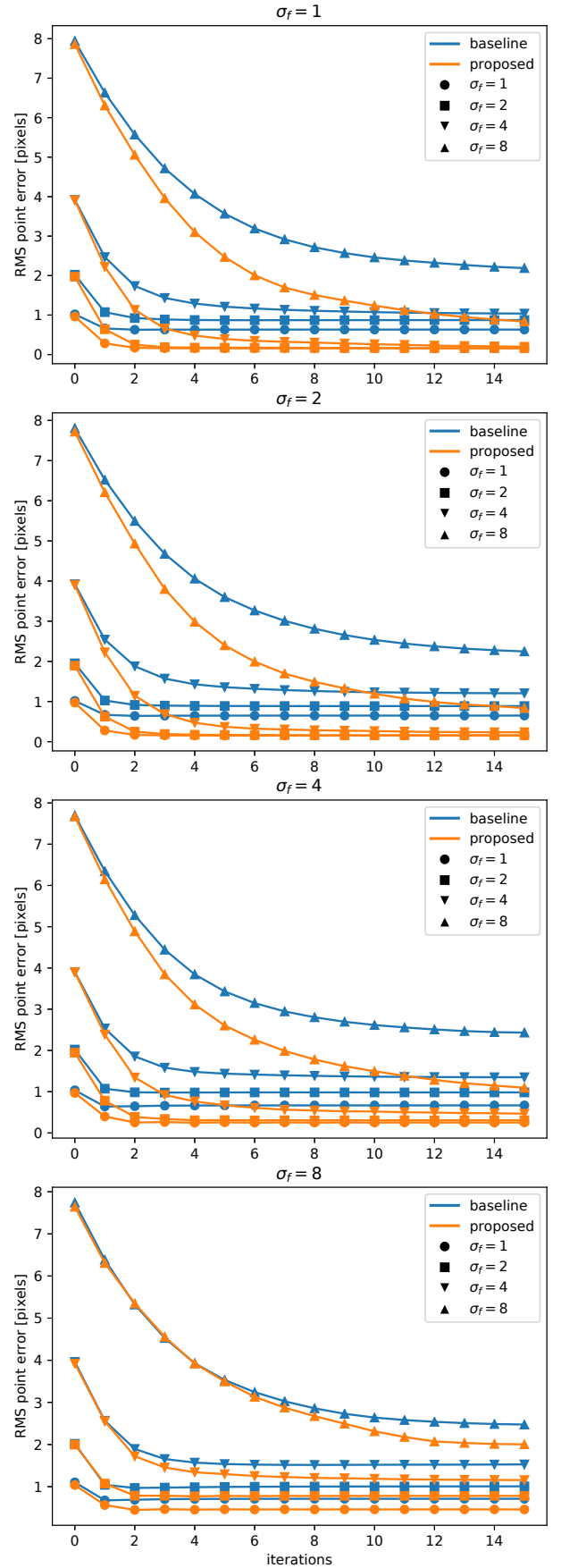


Fig. 10. Average RMS point errors of surface tracking versus number of iterations when interference from a fiducial projection occurs.

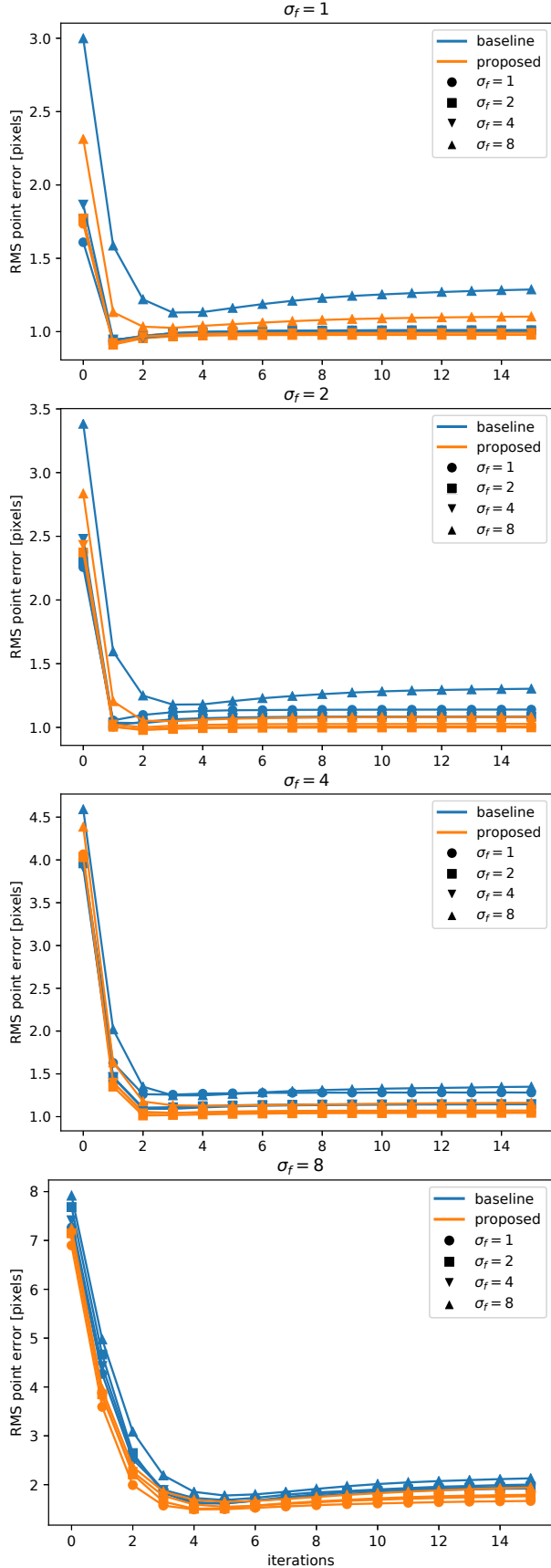


Fig. 11. Average RMS point errors of fiducial tracking versus number of iterations when interference from a fiducial projection occurs.

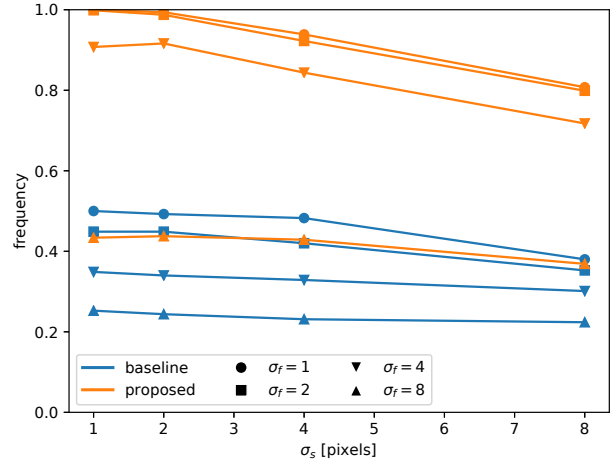


Fig. 12. Frequency of convergence of surface tracking.

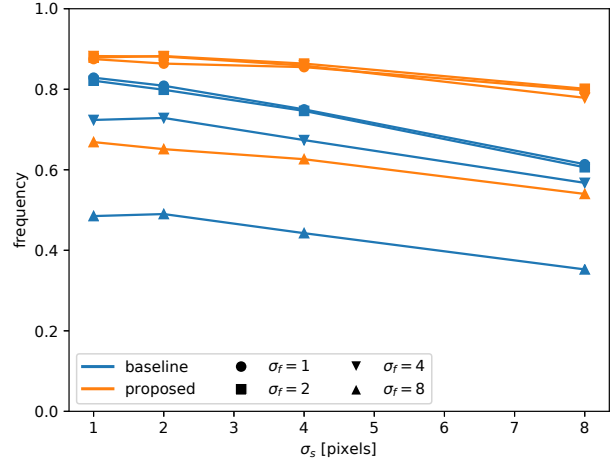


Fig. 13. Frequency of convergence of fiducial tracking.

### 5.3 Results

The convergence rate of the optimization methods in general can be visualized by plotting the errors versus the number iterations. We evaluated the errors based on the root mean square (RMS) errors of the four corner point positions from the ground truth positions. First, we show the results when there was no projection interference to see the basic performance of the baseline (plain ESM) and the proposed methods for a common planar target tracking problem. We used the all-projector-pixels-on images for tracking during these tests. Fig. 8 shows the evolution of the average RMS point errors with respect to the number of iterations, where the trials that diverged were excluded from the average as applied by Baker and Matthew [4]. A trial is said to have diverged when the final RMS error is greater than the initial RMS error.

Another metric for evaluation is the frequency of convergence, which is the number of successful trials that have converged divided by the number of trials. A trial is said to have converged when the final RMS error is smaller than 1.0 pixel. Fig. 9 shows the results when no projection interference occurs.

Fig. 8 and Fig. 9 show that both the baseline and the proposed method work well for surfaces without interfering light, although the proposed method performs marginally worse because the number of pixels that participate in optimization is smaller owing to the pixel selection.

We now move on to the results regarding our primary concern. Fig. 10 shows the average RMS point errors in the surface tracking versus the number of iterations when there was interference by a fiducial

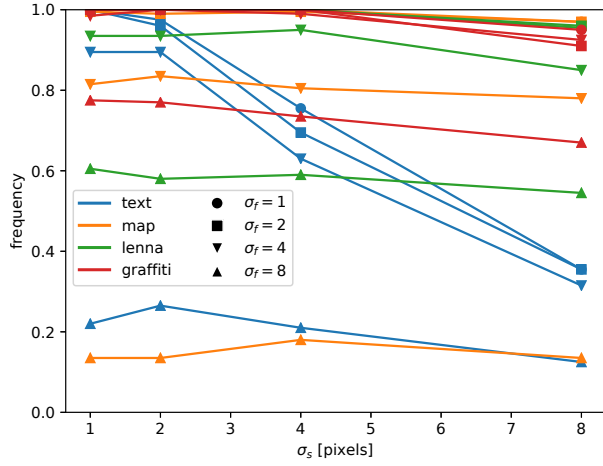


Fig. 14. Frequency of convergence of surface tracking with respect to different surface textures.

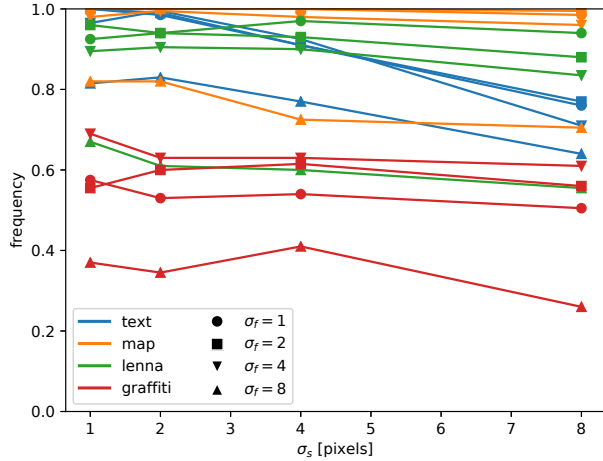


Fig. 15. Frequency of convergence of fiducial tracking with respect to different surface textures.

projection for a different  $\sigma_f$ . In contrast to the case without a projection interference, the plots clearly show that the proposed method performs better and that the convergence rates of the proposed method for  $\sigma_f \leq 4$  are comparable to those without interference. When  $\sigma_f$  is as large as 8, the performance decreases significantly and the average RMS errors behave similarly to those of the baseline method. This is because the assumption of a small inter-frame motion is violated.

Fig. 11 shows the evolution of the average RMS point errors in fiducial tracking with respect to the number of iterations for a different  $\sigma_f$ . The averages here include only those trials in which both the surface tracking and fiducial tracking did not diverge, because the success of surface tracking is a prerequisite for that of fiducial tracking. Also note that the baseline and the proposed methods are the same after the fiducial tracking starts, namely, both simply execute a plain ESM method. The only difference between them is the input image, which is affected by the surface tracking result. The results show that the fiducial tracking converges quickly as a whole with both methods. Although the results may appear to indicate that the proposed method performs consistently better, discretion should be applied. Because the projector control used to display the fiducial patterns was applied using the estimated  $\hat{H}_{pc}$ , the “ground truth” positions of the fiducial corners possibly contained small inevitable bias errors. This can be seen from the fact that the final average RMS error was approximately 1.0 pixel even for the best performing case.

Fig. 12 and Fig. 13 show the frequency of convergence of the surface and fiducial tracking, respectively. Because the final fiducial tracking

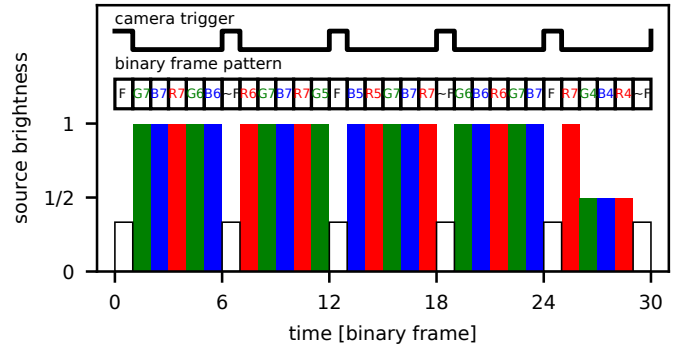


Fig. 16. A sequence of light source and binary frame switching to represent a 4-bit color image with periodically inserted fiducial patterns. Binary frames are specified by symbols, such as R7, which means the 7th bit (i.e., MSB) of the red channel. Symbols F and  $\sim F$  specify the complementary pair of fiducial patterns.

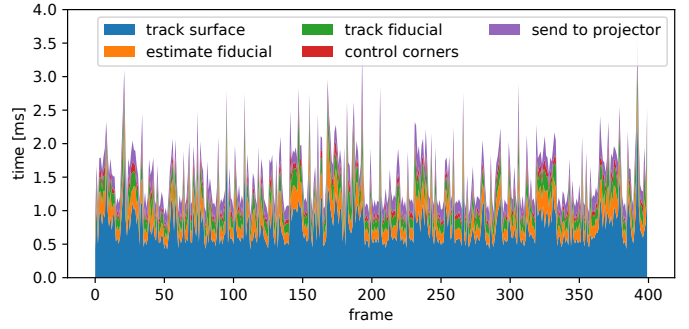


Fig. 17. Stacked plots of the processing time in a sequence of 400 consecutive camera frames.

errors can be large for the reason described above, a trial of the fiducial tracking is said to have converged if the final RMS error is smaller than 1.5 pixels.

The results indicate that the frequency of convergence of the proposed method are almost equally good as long as  $\sigma_f \leq 4$ , although fiducial tracking seems to be more challenging than surface tracking. In contrast to the convergence rate results of the fiducial tracking, in which the rates achieved by both methods are comparable, the difference between the baseline and the proposed methods is clearly significant with respect to frequency of convergence of the fiducial tracking, as well as the surface tracking.

Finally, we examined the influence of different surface textures on the frequency of convergence. Fig. 14 shows the results of the surface tracking, whereas Fig. 15 shows those of the fiducial tracking. These results suggest that the performance depends significantly on the surface texture. The surface tracking is relatively easy with the Lenna and Graffiti surfaces. By contrast, Text and a Map are likely challenging because they contain fine-grained textures for which large displacements are difficult to deal with using iterative alignment methods. This is particularly the case with a Text surface, in which the frequency of convergence rapidly decreases with an increase in  $\sigma_s$ . In contrast, for fiducial tracking, Lenna and Graffiti are rather challenging. This is likely because of the low reflectance of these surfaces and can be overcome by increasing the brightness of the fiducial patterns at the sacrifice of the contrast of the video content.

## 6 DYNAMIC PROJECTION MAPPING RESULTS

We implemented the proposed tracking projection algorithm and tested it for various surfaces with different content.

To encode a video content with a DMD projector presenting 2,400 binary frames per second, 40 binary frames are available for a video frame at 60 fps, although we do not need to be so strict about this,



and more or fewer binary frames can participate in the encoding of an image unless dropped video frames or duplications are fatal for the applications of interest. Because we reserve 1/6 of the binary frames for the fiducial patterns, approximately 33 binary frames are available to represent a video content. This is sufficient for representing an 8-bit full color image if we intensively utilize the light source modulation technique, for which the availability of 24 binary frames is the minimal requirement. However, herein we employ a 4-bit color representation in favor of better light utilization. The employed binary frame sequence in our experiment is shown in Fig. 16, although the choice is not limited to this.

To achieve real-time tracking at 400 fps, we used a parallelized implementation [14] of the ESM algorithm using Intel AVX instructions and multithreading with OpenMP. We set the size of the surface template to a pixel resolution of  $112 \times 112$  and that of the fiducial template to  $48 \times 48$ . The number of iterations was set to 8 and 5 for the surface and fiducial tracking, respectively. Fig. 17 shows stacked plots of the processing time of a tracking projection sequence on a laptop PC with an Intel Core-i7 7600U (2.9 GHz) and 16 GB of RAM running Microsoft Windows 10 Professional.

### 6.1 Tracking Control

Fig. 18, Fig. 19 and Fig. 20 show the results of the tracking control for various types of manual surface motions, which include a circular motion at approximately 4 Hz, vertical shaking at approximately 6 Hz, and spinning about the vertical axis at approximately 4 Hz, respectively. The  $x$  and  $y$  plots with respect to time show trajectories of the upper-left corners of the surface area and the fiducial in the camera image. The RMS point errors between the four corresponding pairs of corners are also shown. Overall, the results indicate that the proposed tracking projection method works quite well in that RMS errors of the corner positions are within 2 pixels most of the time.

It should be noted that these plots are based on the results of visual tracking, which themselves may not be accurate, and hence it is difficult to tell exactly whether the errors are caused by the visual tracking or the tracking control of the projection. However, it is possible to conjecture the reasons for particular cases. For example, all three plots exhibit a periodic variation of the RMS errors corresponding to their periodic motions. We see larger errors in Fig. 18 and Fig. 19 when the movement speed is high, and these seem to have been caused by tracking control errors. In contrast, we see a constant fluctuation of errors in Fig. 20, and their marginal increase when the surface was inclined against the camera. These errors seem to have been caused mainly by visual tracking errors owing to the challenging conditions rather than the tracking control.

### 6.2 Video Content Mapping

This subsection presents snapshots of video content mapping demonstrations. The supplemental video of these scenes shows that the proposed method enables a fairly quick adaptation of the content onto fast moving surfaces.

Fig. 1 shows snapshots from an external video camera that captured the scenes of the projection mapping of the video content. The top row shows a scene in which a rotating logomark of ISMAR2019 was mapped onto a fast-moving printed CFP. The bottom row shows a similar scene with an animation video, where the tracking camera on the left hand side and the surface were being moved by hand, demonstrating that our approach does not rely on a projector-camera calibration.

We also present several application-suggestive examples of video content mapping in Fig. 21. Fig. 21 (a) and (b) show the results of sticking a related video clip and a 3D animation clip onto printed research paper and a book page, respectively. Fig. 21 (c) shows an example of annotating a map using anchors. Through user interaction, a new anchor mark can be placed on a surface point, and the anchors remain stuck to the point even if the surface moves.

Finally, Fig. 21 (d) shows an example of projection mapping on a guitar body. The waveform and spectrum of live sound retrieved by a PC microphone were visualized as mapped content. This demonstration exemplifies a limitation of the proposed approach used to carry out

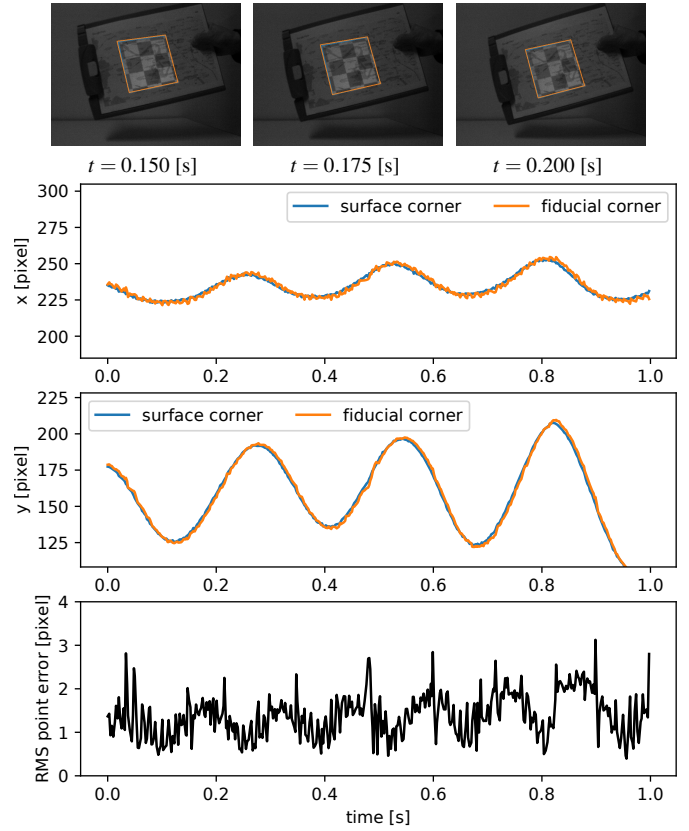


Fig. 18. The tracking projection results when a surface was in circular motion. The top row shows examples of tracking the camera images. The middle two rows present the tracked trajectories. The bottom row shows the RMS error between the corresponding four corners of the surface and the fiducial areas.

markerless surface tracking. Because of the challenging nature of the guitar body surface (maple veneer coated with polyurethane) as a visual tracking target, the tracking was not satisfactorily accurate and was prone to tracking loss.

## 7 LIMITATIONS AND DISCUSSION

### 7.1 Impact on Content Visibility

The proposed approach compromises the contrast of the visible video content through the insertion of fiducial patterns. The decrease in the highest brightness owing to this compromise can be overcome using stronger light sources, although the increase in the black level may occasionally limit the content design. This is significantly visible in Fig. 21 (c), where the solid-color rectangle is not a part of the content but the result of the increase in black level. This effect can be suppressed by lowering the light source intensity only when the fiducial binary frames are illuminated; however, this will necessitate a higher-sensitivity camera to maintain stable fiducial tracking.

Another issue stemming from the inserted fiducials is the possibility of artifact perception. Although naïve viewers can barely notice the existence of fiducials in video content through our implementation, a viewer having knowledge regarding the underlying mechanism can occasionally notice the chessboard boundary by looking closely, particularly when the surface and content are not texture-rich and are close to a solid color. A possible way to work around these contrast and artifact problems is to introduce an infrared projector light source instead of a white light, although the emissions of infrared light may interfere with other peripheral systems using infrared such as motion capture and communication apparatuses.



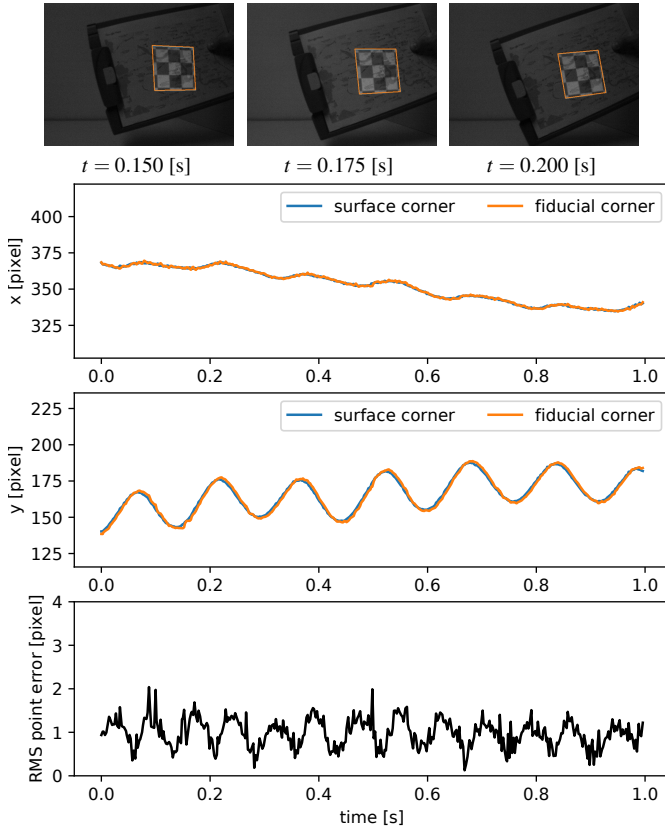


Fig. 19. Tracking projection results when a surface was vertically shaken.

## 7.2 Dependency on Surface Textures

Although the dependency of tracking on the video content has been completely removed, the proposed approach still suffers inherently from a dependency on the surface textures. This approach is of course not applicable to a solid-color surface with no texture. Note, however, that it is possible to combine the methods assuming a solid-color surface and a known shape [12, 13, 26] with the imperceptible fiducial pattern approach, which is rather easy to achieve.

Even if the surface textures are available, because only a subset of pixels is used for surface tracking, we should note that there can be unfortunate situations in which the pixels chosen for tracking do not offer sufficiently rich textures.

## 7.3 Assuming a Planar Target

This paper has focused on tracking a projection onto a planar surface. Generalization to non-planar surfaces is not impossible because direct alignment methods in general are applicable to non-planar objects. For example, an extension to the ESM algorithm has been proposed [28]. However, we should note that the proposed method uses a subset of pixels for optimization. The surface points at the unchosen pixels are not measured, and we therefore must rely on interpolation. For unknown or deformable shapes, we will require extra assumptions such as the spatial smoothness or known dynamics.

The fiducial patterns may also need to be redesigned, particularly when the surface shape is complicated, because the trackability of a pattern with a direct alignment method is affected by the distortion of the pattern observed from the camera view, and the simple pattern design used in this paper may not be sufficient.

## 7.4 Necessity for Special Hardware

The proposed approach is built upon the availability of a high-speed projector-camera pair. This is partly in order to ensure a quick adaptation to fast motion and to enable the tracking algorithm to operate by keeping the image displacement between consecutive frames small.

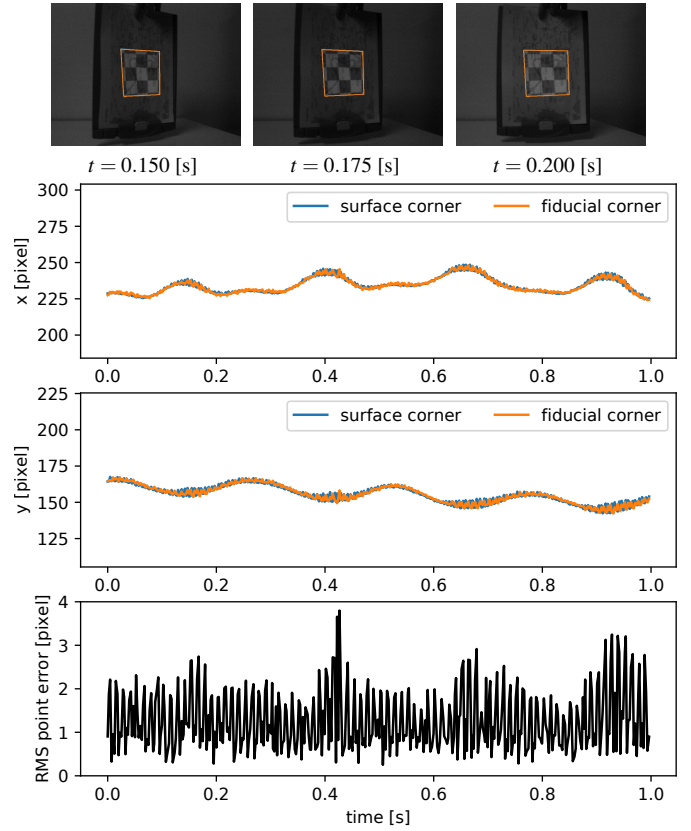


Fig. 20. Tracking projection results when a surface was spinning about the vertical axis.

The necessity for special hardware may sound limiting, but we believe that low-latency camera-projector feedback is essentially required for dynamic projection mapping applications.

It should be noted that the proposed algorithm can be used with different types of high-speed projection systems if they have a real-time rendering capability for high frame rate images as well as synchronization with the camera, although we believe the architecture adopted in our implementation is well suited for consumer-level applications.

## 8 CONCLUSION

This paper described an approach to achieve a fast projection mapping of video content onto a markerless planar surface using an uncalibrated projector-camera pair. A closed-loop alignment has been achieved by inserting fiducial patterns into the binary frame sequence of a DMD projector, which are designed to enable surface tracking and fiducial tracking simultaneously from a single camera image. It was found that 400-fps visual feedback control with the compensation of a one camera frame delay, without modeling the target dynamics, works well in enabling a quick adaptation of content onto fast moving surfaces. In a future study, we aim to tackle some of the limitations described in Sect. 7, including an extension to non-planar surfaces and an improvement of the content visibility by redesigning the fiducial patterns when considering human visual characteristics.

## ACKNOWLEDGMENTS

Part of this work was supported by JST ACCEL JPMJAC1601 and JSPS Grant-in-Aid 19H04146, 16H02853, and 16H06536.

## REFERENCES

- [1] S. Audet, M. Okutomi, and M. Tanaka. Direct image alignment of projector-camera systems with planar surfaces. In *23rd IEEE Conference on Computer Vision and Pattern Recognition (CVPR2010)*, pp. 303–310, 2010.

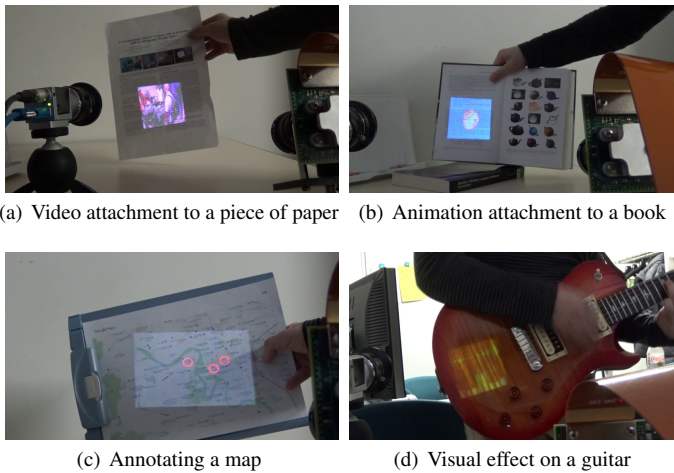


Fig. 21. Snapshots of application-suggestive examples.

- [2] S. Audet, M. Okutomi, and M. Tanaka. Augmenting moving planar surfaces robustly with video projection and direct image alignment. *Virtual Reality*, 17:157–168, 2013.
- [3] S. Baker, R. Gross, T. Ishikawa, and I. Matthews. Lucas-Kanade 20 years on: A unifying framework: Part 2. CMU Robotics Institute Tech. Rep. CMU-RI-TR-03-01, 2003.
- [4] S. Baker and I. Matthews. Lucas-Kanade 20 years on: A unifying framework. *Int. J. Comput. Vis.*, 56(3):221–255, 2004.
- [5] S. Benhimane and E. Malis. Homography-based 2D visual tracking and servoing. *Int. J. Robotics Res.*, 26(7):661–676, 2007.
- [6] A. H. Bermanno, M. Billeter, D. Iwai, and A. Grundhöfer. Makeup lamps: Live augmentation of human faces via projection. *Comput. Graph. Forum*, 36(2):311–323, 2017.
- [7] D. Cotting, M. Naef, M. Gross, and H. Fuchs. Embedding imperceptible patterns into projected images for simultaneous acquisition and display. In *3rd IEEE and ACM International Symposium on Mixed and Augmented Reality (ISMAR2004)*, pp. 100–109, 2004.
- [8] F. Dellaert and R. Collins. Fast image-based tracking by selective pixel integration. In *ICCV1999 Workshop on Frame-Rate Vision*, 1999.
- [9] S. Garrido-Jurado, R. Muñoz-Salinas, F. J. Madrid-Cuevas, and M. J. Marí-Jiménez. Automatic generation and detection of highly reliable fiducial markers under occlusion. *Pattern Recognit.*, 47(6):2280–2292, 2014.
- [10] A. Grundhöfer, M. Seeger, F. Hantsch, and O. Bimber. Dynamic adaptation of projected imperceptible codes. In *6th IEEE and ACM International Symposium on Mixed and Augmented Reality (ISMAR2007)*, pp. 181–190, 2007.
- [11] T. Hiraki, S. Fukushima, and T. Naemura. Phygital field: An integrated field with a swarm of physical robots and digital images. In *9th ACM SIGGRAPH Conference and Exhibition on Computer Graphics and Interactive Techniques in Asia (SIGGRAPH Asia 2016 Emerging Technologies)*, 2016. Article no.2.
- [12] T. Johnson and H. Fuchs. Real-time projector tracking on complex geometry using ordinary imagery. In *IEEE International Workshop on Projector-Camera Systems (ProCams2007)*, 2007.
- [13] S. Kagami and K. Hashimoto. Sticky projection mapping: 450-fps tracking projection onto a moving planar surface. In *8th ACM SIGGRAPH Conference and Exhibition on Computer Graphics and Interactive Techniques in Asia (SIGGRAPH Asia 2015 Emerging Technologies)*, 2015. Article no.23.
- [14] S. Kagami and K. Hashimoto. High-frame-rate region-based visual tracking on CPU: An implementation perspective. In *IEEE/SICE International Symposium on System Integration (SII2016)*, pp. 562–567, 2016.
- [15] S. Kagami and K. Hashimoto. A full-color single-chip-DLP projector with an embedded 2400-fps hom ography warping engine. In *45th International Conference and Exhibition on Computer Graphics and Interactive Techniques (SIGGRAPH2018 Emerging Technologies)*, 2018. Article no.1.
- [16] G. Klein. Registration on Hololens. In *16th IEEE International Symposium on Mixed and Augmented Reality (ISMAR2017)*, Keynote Talk, 2017.
- [17] T. Kusanagi, S. Kagami, and K. Hashimoto. Lightning markers: Synchronization-free single-shot detection of imperceptible ar markers embedded in a high-speed video display. In *16th IEEE International Symposium on Mixed and Augmented Reality (ISMAR2017)*, Posters, pp. 229–234, 2017.
- [18] P. Lincoln, A. Blate, M. Singh, T. Whitted, A. State, A. Lastra, and H. Fuchs. From motion to photons in 80 microseconds: Towards minimal latency for virtual and augmented reality. *IEEE Trans. Vis. Comput. Graph.*, 22(4):1367–1376, 2016.
- [19] I. E. McDowall, M. T. Bolas, P. Hoberman, and S. S. Fisher. Snared illumination. In *31st International Conference on Computer Graphics and Interactive Techniques (SIGGRAPH2004 Emerging Technologies)*, p. 24, 2004.
- [20] L. Miyashita, Y. Watanabe, and M. Ishikawa. MIDAS projection: Markerless and modelless dynamic projection mapping for material representation. *ACM Trans. Graph.*, 37(6), 2018. Article no.196.
- [21] H. Naik, F. Tombari, C. Resch, P. Keitler, and N. Navab. A step closer to reality: Closed loop dynamic registration correction in SAR. In *14th IEEE International Symposium on Mixed and Augmented Reality (ISMAR2015)*, Posters, pp. 112–115, 2015.
- [22] T. Nakamura, F. de Sorbier, S. Martedi, and H. Saito. Calibration-free projector-camera system for spatial augmented reality on planar surfaces. In *21st International Conference on Pattern Recognition (ICPR2012)*, pp. 85–88, 2012.
- [23] G. Narita, Y. Watanabe, and M. Ishikawa. Dynamic projection mapping onto deforming non-rigid surface using deformable dot cluster marker. *IEEE Trans. Vis. Comput. Graph.*, 23(3):1235–1248, 2017.
- [24] W. Oshiro, S. Kagami, and K. Hashimoto. Perception of motion-adaptive color images displayed by a high-speed dmd projector. In *IEEE VR 2019 Workshop on Perception-driven Graphics and Displays for VR and AR (PerGraVAR2019)*, 2019.
- [25] R. Raskar, G. Welch, M. Cutts, A. Lake, L. Stesin, and H. Fuchs. The office of the future: A unified approach to image-based modeling and spatially immersive displays. In *25th Annual Conference on Computer Graphics and Interactive Techniques (SIGGRAPH 1998)*, pp. 179–188, 1998.
- [26] C. Resch, P. Keitler, and G. Klinker. Sticky projections – a model-based approach to interactive shader lamps tracking. *IEEE Trans. Vis. Comput. Graph.*, 22(3):1291–1301, 2016.
- [27] C. Siegl, M. Colaiani, L. Thies, J. Thies, M. Zollhöfer, S. Izadi, M. Stamminger, and F. Bauer. Real-time pixel luminance optimization for dynamic multi-projection mapping. *ACM Trans. Graph.*, 34:6, 2015. Article no.237.
- [28] G. Silveira and E. Malis. Unified direct visual tracking of rigid and deformable surfaces under generic illumination changes in grayscale and color images. *Int. J. Comput. Vis.*, 89(1):84–105, 2010.
- [29] G. Suzuki, N. Yamaguchi, S. Nakamura, and H. Chiba. Mobile interaction using steganographic image on mobile display. In *10th International Conference on Human Computer Interaction with Mobile Devices and Services (MobileHCI2008)*, pp. 507–510, 2008.
- [30] K. Warwick and D. Rees. *Industrial Digital Control Systems*. Peter Peregrinus, London, 1988.
- [31] K. D. D. Willis, I. Poupyrev, S. E. Hudson, and M. Mahler. SideBySide: Ad-hoc multi-user interaction with handheld projectors. In *24th ACM Symposium on User Interface Software and Technology (UIST2011)*, pp. 431–440, 2011.
- [32] G. Yamamoto, L. Sampaio, T. Taketomi, C. Sandor, H. Kato, and T. Kuroda. Imperceptible on-screen markers for mobile interaction on public large displays. *IEICE Trans. Inf. & Syst.*, E100D(9), 2017.
- [33] F. Zheng, R. Schubert, and G. Welch. A general approach for closed-loop registration in AR. In *IEEE Virtual Reality Conference (IEEE VR 2013)*, pp. 47–50, 2013.
- [34] F. Zheng, T. Whitted, A. Lastra, P. Lincoln, A. State, A. Maimone, and H. Fuchs. Minimizing latency for augmented reality displays: Frames considered harmful. In *13th IEEE International Symposium on Mixed and Augmented Reality (ISMAR2014)*, pp. 195–200, 2014.
- [35] Y. Zhou, S. Xiao, N. Tang, Z. Wei, and X. Chen. Pmomo: Projection mapping on movable 3D object. In *CHI2016*, pp. 781–790, 2016.